Design and Transformation Control of Triangulated Origami Tessellation: A Network Perspective

Gangshan Jing*, Changhuang Wan*, Ran Dai, and Mehran Mesbahi *Fellow, IEEE*

.

***Abstract*—Origami is known as a traditional art of paper folding. It has attracted extensive attention due to its self-folding mechanism, shape-morphing capability, and deployable structures. This paper develops network-based methods for designing and controlling a three-dimensional (3D) triangulated origami tessellation to approximate multiple surfaces. The desired surfaces are represented by sets of discrete nodes and the origami tessellation to be designed is composed of triangles. Then, the tessellation design problem is formulated as an optimization problem of minimizing the distance between the origami triangle vertices and the discrete nodes subject to developability and rigid-foldability constraints. Solving the resulting optimization problem leads to an origami tessellation with folding states associated with each target surface. To achieve transformation between different shapes, we first leverage graph rigidity theory to define every 3D origami shape uniquely up to translations and rotations. Next, in order to minimize the control efforts, the shape transformation control problem is formulated as an optimal control problem subject to the derived rigidity conditions, whose feasibility is guaranteed by transformability of the origami and controllability of dynamic vertices. Finally, simulation examples for surface approximation are provided to verify the effectiveness of the network-based design and control methods.**

***Index Terms*—Origami tessellation, Network design, Rigidity theory, Optimization**

I. Introduction

ORIGAMI, the ancient art of folding flat paper into diverse shapes, has attracted increasing attention from researchers in both science and engineering [1], [2], [3], [4], [5], [6]. Due to its advantages in reconfigurability and deployment capabilities, there exist many applications of origami-inspired structures, including deployable space structures [7], [8], biomedical devices [9], [10], architecture [11], robots [12] and manipulators [13]. Most of these applications utilize a customized crease pattern to form a desired shape with rigid engineering sheet materials [14]. To design such a crease pattern, kinematics of origami [15], [16], [17] and formulation of crease pattern design problems [18], [19], [20], [21] are two essential topics under investigation.

To analyze the kinematics of origami structures, assumptions on rigid folding motion and zero-thickness have been considered [15]. The rigid folding assumes that all the facets separated by fold lines are rigid. Zero-thickness allows an origami structure to fold along the creases with zeroth-order geometric continuity. Based on these assumptions, rigid folding is defined as a process that folds the rigid facets continuously without deformation. Accordingly, rigid foldability refers to the ability to fold an origami from an initial shape to a target one while preserving the characteristics of a rigid origami, such as distance and angle constraints.

Graph theory is a useful tool for the rigid origami configuration representation and design [22]. It is natural to correspond origami vertices and creases with graph elements. Typically, an origami is modeled as a crease pattern graph where paper creases are modeled as the edges, and intersections of creases are considered as the vertices in a graph. Based on the crease pattern graph, conditions for rigid foldability and the degrees of freedom (DoF) of a single vertex origami have been investigated, including Huzita-Hatori axioms [23], the Maekawa's theorem (developability) [24], and Kawasaki's theorems (flat foldability) [25], [26]. With these rigidity conditions, Wu and You [17] described the deformation model of rigid origami using quaternions and dual quaternions. Xi and Lien [16] simulated the folding process by modeling rigid origami as a kinematic system with closure constraints. He and Guest in [27] investigated the static rigidity, pre-stress stability, and second-order rigidity of rigid origami structures. When extending to a multi-vertex origami, it has been proven that finding the overlap order for the facets and folding path of a general origami is NP-hard and generally intractable [4], [28]. Hence, most existing approaches for multi-vertex origami have utilized the generalization of single-vertex through a periodic crease pattern or 'tiling' of a flat sheet, known as origami tessellations. The rational periodic design enables a synchronized folding mechanism for a designed structure. Among existing origami tessellation patterns, the *Miura-ori* with four-crease pattern [29] and *waterbombs* with six- or eight-crease pattern [30], [31], [32] are the major origami tessellations that have been widely used in origami designs.

The origami design problem refers to the process of generating a crease pattern that has desired characteristics and can be folded to achieve desired configurations in space [4], [33], [34]. Considering the manufacturability or foldability criterion, various approaches (e.g., [35], [36], [37], [21]) have been proposed for symmetry origami design. However, few efforts have been made to establish a design or control paradigm that uses one designed origami tessellation to match multiple three-dimensional (3D) surfaces by controlling the folding process. Designing origami tessellations to approximate mul-

This research is supported in part by NSF grants CPS-2201568 and CPS-2201612

Gangshan Jing is with the School of Automation, Chongqing University, Chongqing, 400044, PRC

Changhuang Wan is with the Aerospace Engineering Department, Tuskegee University, Tuskegee, AL, 36088 USA

Ran Dai is with the School of Aeronautics and Astronautics, Purdue University, West Lafayette, IN, 47907, USA

Mehran Mesbahi is with the Department of Aeronautics and Astronautics, University of Washington, Seattle, WA, USA

*The first two authors contributed equally to this work.

tiple 3D surfaces is a challenging task that requires careful consideration of how the folds interact with each other to create a cohesive pattern. This becomes more difficult when surfaces have different curvatures or shapes that are difficult to represent with a single origami tessellation. Additionally, the multiple surfaces must intersect smoothly to create a seamless transition, and as the number of surfaces increases, the complexity of the design increases, making it harder to maintain the paper's structural integrity. This paper proposes a novel framework from the network perspective for origami tessellation design and control to match multiple 3D surfaces. The design problem is to minimize the distances between the designed origami vertices and discrete nodes on target surfaces. Solving the resulting problem via nonlinear programming (NLP) leads to an optimal design result with vertices locations and folding status associated with each target surface.

Achieving different target surfaces from a designed origami tessellation relies on controlling the folding process, referred to as transformation control here. This paper aims to minimize the control efforts when transforming the designed origami from one target surface to another. To guarantee the feasibility of transforming between two target shapes, we introduce a new notion of transformability. To allow flexibility while minimizing the control efforts with guaranteed transformability, we leverage graph rigidity theory on triangulated frameworks [38] to define a unique shape up to translations.

Overall, this paper develops a network-based systematic approach to designing origami tessellation and controlling the shape transformation to match multiple 3D surfaces. As an emerging topic in the area of network-based design and control, our main contributions can be summarized as follows: (i) modeling the origami design problem as a nonlinear optimization problem to minimize the difference between origami vertices and discrete nodes on the target surfaces subject to distance constraints and angle constraints; (ii) employing a weak rigidity function containing information of edge lengths and angle values to guarantee transformability in the transformation process; and (iii) formulating the origami transformation control problem as an optimally constrained control problem to minimize the control efforts with local shape preservation constraints.

Compared with state-of-the-art methods for origami design and transformation control, the main features of our work include the following three folds: (i) extending single-surface approximation to multi-surface approximation using one designed origami tessellation; (ii) introducing the concept of transformability of origami and proposing a novel formulation for seeking a transformation approach with minimum control effort; (iii) leveraging graph rigidity theory to support the feasibility of transformation control, which has not been established in existing origami transformation control approaches.

This paper is organized as follows. Section II introduces basic theorems for flat-foldable origami. Section III describes the geometry of unit six-crease origami and tessellations. Then, a framework for designing origami crease patterns to approximate multiple surfaces is introduced in Section IV. To examine the transformability of the designed origami, Section V proposes a new rigidity function to uniquely define the 3D shape of a designed origami. Based on the developed rigidity theory, modeling of the transformation control problem is described in Section VI. Section VII presents an example to validate the effectiveness of the proposed design and control methods. Conclusions are addressed in Section VIII.

II. Preliminaries

An origami configuration can be modeled as a planar straight-line graph that can be drawn so that the straight-line edges only intersect at the vertex points. An origami diagram that consists of all the creases, usually rendered into one image, is called the crease pattern, denoted as $\mathcal{C}$. A single vertex origami only has one intersection of all creases. The angle between two adjacent creases is named the sector angle. For the single vertex crease pattern, the degree of the vertex is the number of edges joining it, which also equals the number of sector angles around the vertex.

1) Developability of origami: An origami object is usually folded from a flat paper sheet to a specific 3D shape. Under the flat sheet status, it is obvious that the sector angles around a vertex sum to 2π [24]. In fact, this constraint, known as Kawasaki's theorem or developability of an origami, holds all the time during the folding process. For a multi-vertex crease pattern, the developability constraint is given by

$$\sum_{i=1}^{n} \varphi_{i,j} = 2\pi,\ j \in \mathcal{V}_{in}, \tag{1}$$

where $\mathcal{V}_{in}$ is the set of the interior vertex, n is the degree of the interior vertex, and $\varphi_{1,j}, \varphi_{2,j}, \ldots, \varphi_{n,j}$ are the sector angles around the jth interior vertex, oriented clockwise.

2) Flat-foldability of origami: It has been proven that a single-vertex crease pattern is flat-foldable if and only if the vertex has an even degree and the sum of the odd angles is equal to that of the even angles [24], i.e.,

$$\sum_{i=1}^{n/2} \varphi_{2i-1,j} = \sum_{i=1}^{n/2} \varphi_{2i,j} = \pi,\ \forall\, \varphi_{i,j} \in (0, \pi) \tag{2}$$

3) Mountain-Valley (MV) assignment: For an origami structure, a crease can be folded in two ways: *mountain* folding that bends the crease in a convex direction, and *valley* folding that bends the crease in a concave direction. An example of MV assignment is shown in Fig. 1 (a), where the three red lines represent the mountains, and the blue line denotes the valley.

Let M be the number of mountain folds and V be the number of valley folds. A given crease pattern often has more than one possible MV assignment combination that differs by alternating the mountain or valley folds. Mathematically, an MV assignment of a crease pattern can be considered as a mapping function $\kappa : \mathcal{C} \to \{M, V\}$. For a single vertex crease pattern, the following result holds for the MV assignment.

Theorem II.1. *[Theorem 12.2.3 in [39]] For a flat-foldable vertex with M mountain folds and V valley folds, the difference of M and V is always 2, i.e., $|M - V| = 2$.*

Although the developability, the flat-foldability, and the MV assignment theorem stated above are for an n-degree single vertex origami, we will consider a periodic origami crease

pattern or an origami tessellation, such that all these theorems for a single vertex origami structure can be extended to a multi-vertex origami structure.

III. Six-crease Origami Tessellations

A. Generic Six-crease Origami Base

This paper focuses on the crease pattern design using generic six-crease bases. Then, the origami tessellation is to periodically tile the six-crease bases. A generic six-crease base is shown in Fig. 1 (b), where the dash lines represent the creases of the origami, the solid lines are the boundaries of origami, the red point V_0 is the interior vertex, $V_1, V_2, \cdots, V_6$ are the boundary vertices, A_i denotes the section facet between two adjacent creases, $\varphi_1, \varphi_2, \ldots, \varphi_6$ are the sector angles around the interior vertex V_0, and $\theta_1, \theta_2, \ldots, \theta_6$ denote the folding angles along each crease. Typically, the dihedral angle between two adjacent facets connected by the crease is utilized to calculate the corresponding folding angle. To be specific, the folding angle of the ith crease is computed by,

$$\theta_i = \tau_i \cos^{-1}\left(\frac{(\mathbf{p}_i \times \mathbf{p}_{i-1}) \cdot (\mathbf{p}_i \times \mathbf{p}_{i+1})}{\|\mathbf{p}_i \times \mathbf{p}_{i-1}\| \cdot \|\mathbf{p}_i \times \mathbf{p}_{i+1}\|}\right) \tag{3}$$

where $\mathbf{p}_i$ denotes the vector from V_0 to V_i, and τ_i is defined by

$$\tau_i = \begin{cases} 1, & \text{for mountain fold,} \\ -1, & \text{for valley fold.} \end{cases} \tag{4}$$

In other words, $\theta_i \in [-180°, 0°]$ is the folding angle range for valley fold, while $\theta_i \in [0°,\ 180°]$ is the folding angle range for mountain fold. When a generic six-crease base in Fig. 1 (b) is rigidly flat-foldable, the sector angles around the interior vertex must satisfy the flat-foldability constraint in (2) for $n = 6$.

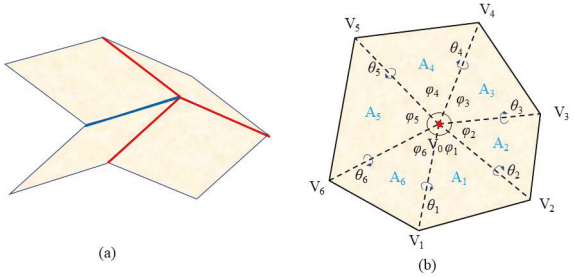

Fig. 1: (a) Mountain-Valley folding example of a degree-4 origami; (b) A generic six-crease base

B. Geometry of Six-crease Origami Tessellation

To generate the origami tessellation using six-crease bases, the crease pattern base should be axis-symmetric such that it can be periodically tiled using a paper sheet. Consider a crease pattern made by tessellating a generic symmetric six-crease base with $col = 5$ columns and $row = 6$ rows, shown in Fig. 2 (a), then the origami tessellation contains multiple triangles with $n = 2 * col * row + col + 3 * row + 1$ vertices and $e = 6 * col * row + 5 * row + col$ edges.

The six-crease origami tessellation in Fig. 2 (a) is made of three types of interior vertices or bases, A, B, and C, which are enlarged in Figs. 2 (b)-(d), respectively. Each of them contains six triangles. Without loss of generality, let the creases $V_{A0}V_{A1}$ and $V_{A0}V_{A4}$ be collinear, and $V_{A0}V_{A4}$ be the axis of symmetry for type A origami base in $\mathbb{R}^2$. Then, due to the line symmetry, the sector angles $\varphi_1 = \varphi_6 = \alpha_A$, $\varphi_2 = \varphi_5 = \beta_A$, and $\varphi_3 = \varphi_4 = \gamma_A$. Moreover, combining with the developability and flat-foldability of a rigid origami, we have

$$\alpha_A + \beta_A + \gamma_A = \pi. \tag{5}$$

Similarly, applying the symmetry conditions to the type B and type C vertices leads to $\alpha_B + \beta_B + \gamma_B = \pi$ and $\alpha_C + \beta_C + \gamma_C = \pi$. In addition, it is straightforward that in the triangle $\triangle_{V_{A0}V_{A4}V_{A5}}$, we have

$$\alpha_C + \beta_B + \gamma_A = \pi. \tag{6}$$

Due to the adjacency of unit origami bases of types A, B, and C, the vertex V_{A0} in type A base is overlapping with the vertex V_{B2} in type B. The same observations can be found for the vertex pair $\{V_{A5}, V_{B0}\}$.

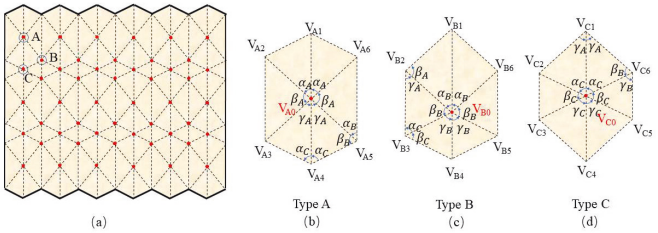

Fig. 2: (a) Crease pattern of six-crease origami tessellation; (b) Type A base; (c) Type B base; (d) Type C base.

Furthermore, when the crease $V_{A2}V_{A3}$ is assumed to be parallel to $V_{A5}V_{A6}$, we have $\alpha_B = \gamma_A$ and $\alpha_C = \gamma_B$. Note that we only have the symmetric constraints on the geometric parameters, i.e., sector angles φ_i, without imposing the symmetric folding constraints on θ_i. In addition, according to Theorem II.1, a generic six-crease base has 2 mountain and 4 valley folds, or vice versa. For example, if we further assume symmetric folding for type A, i.e., $\theta_1 = \theta_4, \theta_2 = \theta_6, \theta_3 = \theta_5$, the folding states of type A with different MV assignments are presented in Fig. 3 (a) and Fig. 3 (b), where the blue and red lines represent the valley and mountain creases, respectively.

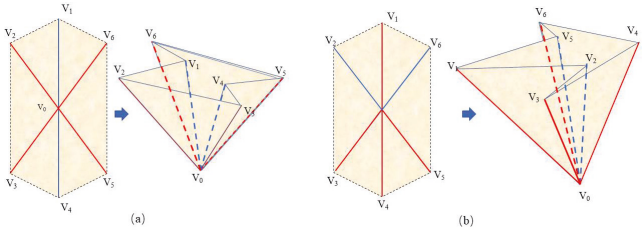

Fig. 3: 2-valley and 4-mountain assignments and the corresponding folding state: (a) V_0V_1 and V_0V_4 are 2-valley creases (b) V_0V_2 and V_0V_5 are 2-valley creases.

C. Kinematics of Origami Folding

For a rigid origami, facets and crease lines are treated as rigid panels and revolute joints, respectively. Then, the kinematics of a rigid single vertex origami is equivalent to the kinematics of a spherical linkage loop with all rotation axes

intersecting at one point [14]. Therefore, an origami rigidly folding around the interior vertex V_0 along the ith crease can be expressed as a rotation matrix using the Denavit-Hartenberg notation, written as

$$\mathbf{T}_{i,i+1}(\varphi_i,\theta_i)=\begin{bmatrix}1 & 0 & 0\\ 0 & \cos\varphi_i & -\sin\varphi_i\\ 0 & \sin\varphi_i & \cos\varphi_i\end{bmatrix}\begin{bmatrix}\cos\theta_i & \sin\theta_i & 0\\ -\sin\theta_i & \cos\theta_i & 0\\ 0 & 0 & 1\end{bmatrix}.$$

The transformation matrix $\mathbf{T}_{i,i+1}$ transforms any vectors in the ith coordinate system to the $(i+1)$th coordinate system. The inverse transformation matrix is denoted by $\mathbf{T}_{i+1,i}$, and $\mathbf{T}_{i,i+1}\mathbf{T}_{i+1,i}=\mathbf{I}_{3\times3}$, where $\mathbf{I}_{3\times3}$ is a 3-by-3 identity matrix. Then, for the loop spherical linkages, there exists a closure equation, expressed as

$$\mathbf{T}_{1,2}\mathbf{T}_{2,3}\mathbf{T}_{3,4}\mathbf{T}_{4,5}\mathbf{T}_{5,6}\mathbf{T}_{6,1}=\mathbf{I}_{3\times3}. \tag{7}$$

Mathematically, (7) implies that after applying the six sequential transformations, it always leads to an identity matrix. When applying (7) to origami folding, it prevents the crease paper from being physically torn by the folding motion. Equivalently, (7) can be rewritten as

$$\mathbf{T}_{\text{diff}}=\mathbf{T}_{1,2}\mathbf{T}_{2,3}\mathbf{T}_{3,4}-\mathbf{T}_{1,6}\mathbf{T}_{6,5}\mathbf{T}_{5,4}=\mathbf{0}_{3\times3}. \tag{8}$$

When the origami tessellation is given, all the sector angles and lengths of edges are fixed and given. Thus, (8) contains nine equations on the six folding angles, θ_i, $i=1,\ldots,6$. Since the elements of a rotation matrix are coupled, (8) reduces to three independent constraints on the folding angles. In other words, only three of the six folding angles are independent, which is consistent with the rigidity analysis of the triangulated framework based on the vertex coordinates in subsection V-C. As a result, the matrix equality constraint in (8) reduces to three scalar equations by letting three matrix elements equal to zero, i.e.,

$$\mathbf{T}_{\text{diff}}(1,2)=0,\ \mathbf{T}_{\text{diff}}(2,3)=0,\ \mathbf{T}_{\text{diff}}(3,3)=0. \tag{9}$$

The solutions to (9) define the configuration space of an interior origami, which is described by the folding angles.

Obviously, since the rotation matrix $\mathbf{T}_{\text{i,i+1}}$ also includes the sector angles, the solutions to (9) vary with different sector angles. In other words, an origami tessellation is capable of forming different desired 3D shapes by assigning the sector angles and setting the crease folding angles subject to (5) and (6). For example, when $\alpha_A=\gamma_A$, $\alpha_C=\alpha_B$, $\gamma_B>90°$, and $\alpha_C>90°$, the crease pattern becomes a symmetric water-bomb origami tessellation, which is shown in Fig. 4.

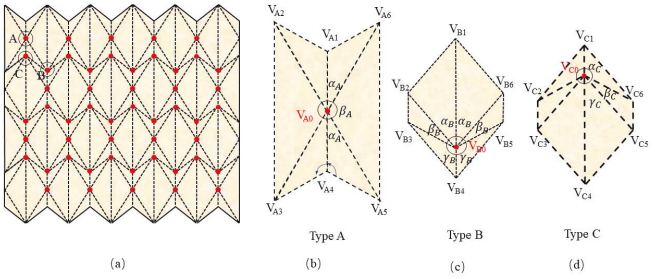

Fig. 4: (a) Symmetric water-bomb tessellation; (b) Water-bomb crease bases

IV. Triangulated Origami Design for Approximating Multiple Target Surfaces

This section presents the design framework for approximating multiple target surfaces based on the six-crease origami tessellation. Due to symmetry, we only consider the vertices on one side of the origami when approximating a given surface. The goal of the origami design is to approximate multiple target surfaces as closely as possible by designing both origami tessellation and the corresponding folding states for each target surface.

The optimal design framework with detailed steps is illustrated in Fig. 5. Firstly, a target surface, denoted by $\mathcal{S}$, is discretized via triangular meshes. Then, the target surface can be represented by intersection points of triangular meshes, denoted by $\mathcal{N}_S$. If there exists a set of vertices $\mathcal{V}_T$ on one side of a partially folded origami such that they coincide with or are close to the discrete nodes in $\mathcal{N}_S$, the target surface is considered to be approximated by the 3D origami. Thus, $|\mathcal{V}_T|=|\mathcal{N}_S|$, where $|\cdot|$ denotes the cardinality of the set '$\cdot$'. For each target surface, such discretization approach will be applied to find its corresponding nodes for surface approximation. Next, an optimization problem is formulated to design the crease pattern and folding angles associated with each target surface such that the distances between $\mathcal{V}_T$ of the designed origami and $\mathcal{N}_S$ on all target surfaces are minimized while satisfying a set of equality constraints, including developability, rigid-foldability, and inequality constraints (e.g., box constraints on crease lengths). The design problem is then classified as a nonlinear optimization problem. Solving the formulated optimization problem via an NLP solver leads to the optimal design result in the form of an origami tessellation and folding states associated with each target surface. The following subsections describe the detailed steps in the design framework.

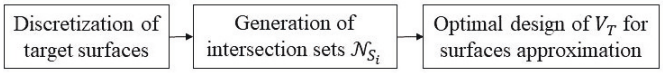

Fig. 5: Framework for origami design

A. Discretization of Target Surfaces

In order to represent a target surface by a set of discrete nodes, the target surface is discretized by triangular meshes. Using the surface in Fig. 6 (a) as an example, the discretized surface is shown in Fig. 6 (b) when discretized by the triangular meshes. The intersection points of the triangular meshes are collected as a set of discrete nodes, $\mathcal{N}_S=\{\mathbf{p}_1,\mathbf{p}_2,\ldots,\mathbf{p}_{|\mathcal{N}_S|}\}$, where $\mathbf{p}_i$, $i=1,\ldots,|\mathcal{N}_S|$, denotes coordinates of an intersection point. As mentioned above, $|\mathcal{V}_T|$ vertices will be assigned to approximate these discrete nodes. Thus, the total number of vertices, n, in the origami tessellation should be larger than $|\mathcal{V}_T|$. Moreover, to ensure the origami is capable of approximating these discrete nodes, the degree of freedom (DoF) of tessellation should satisfy that $DoF-6>3|\mathcal{N}_S|$, where 6 refers to the DoF of three rigid translations and three rigid rotations. The DoF analysis of origami tessellations will be further explained in Section V-C.

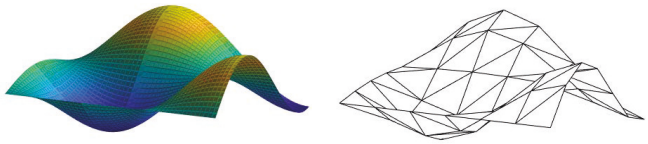

(a) An arbitrary surface (b) Triangular meshes

Fig. 6: Discretization of an arbitrary target surface

B. Formulation of Origami Design Problem

In order to approximate multiple target surfaces, an optimization problem will be formulated in this subsection. The design variables, objective function, and equality and inequality constraints of the optimal design problem are discussed below, respectively.

1) Objective function and design variables: To evaluate the precision of approximating a target surface $\mathcal{S}$ using an origami tessellation, the distance between the discrete nodes on the target surface and the corresponding vertices of the designed origami is referred as a performance index, defined as

$$d_H(\mathcal{N}_S, \mathcal{V}_T) = \sum_{i=1}^{|\mathcal{N}_S|} w_i \|\mathbf{p}_i - \mathbf{x}_i(\mathcal{V}_T)\|, \tag{10}$$

where $\mathbf{x}_i(\mathcal{V}_T) \in \mathbb{R}^3$ denotes the position vector of the ith vertex in $\mathcal{V}_T$ of a partially folded origami, and w_i is the weighting factor. As $\mathbf{x}_i(\mathcal{V}_T), i = 1, 2, \cdots, |\mathcal{N}_S|$, have varying magnitudes, $\|\mathbf{p}_i - \mathbf{x}_i(\mathcal{V}_T)\|$ will also have different magnitudes. By introducing the weighting factor w_i associated with $\|\mathbf{p}_i - \mathbf{x}_i(\mathcal{V}_T)\|$, adjustments can be made to the approximate shape, resulting in an improved approximation accuracy. Then, in the optimal design problem, the objective is to minimize $d_H(\mathcal{N}_S, \mathcal{V}_T)$ by finding vertex locations of the designed origami. To approximate multiple surfaces, the objective function is formulated as

$$\min\ d_{\max} = \max_{i=1}^{q} d_H(\mathcal{N}_{Si}, \mathcal{N}_{Ti}) \tag{11}$$

where q is the number of target surfaces. When approximating multiple surfaces using one designed origami tessellation, the vertex sets $\mathcal{V}_{T1}, \ldots, \mathcal{V}_{Tq}$ can be different. Therefore, the corresponding coordinate sets $\mathbf{x}^1, \mathbf{x}^2, \cdots, \mathbf{x}^q \in \mathbb{R}^{|\mathcal{V}|\times 3}$ for all vertices may also be different. In addition to the coordinates of all vertices, the sector angles $\boldsymbol{\varphi}$ are required to determine the entire origami tessellation. With a designed origami tessellation, matching every target surface is realized by changing the folding angles. Therefore, the sector angles $\boldsymbol{\varphi}$, folding angles $\boldsymbol{\theta}$, and the coordinates of vertices $\mathbf{x}^1, \mathbf{x}^2, \cdots, \mathbf{x}^q$ are considered as designed variables.

2) Equality constraints: To satisfy the general properties of origami, several sets of equality constraints, including the developability and the rigid foldability, are considered in the design problem formulation, expressed as

$$h_{\text{develop},j}(\boldsymbol{\varphi}) = 2\pi - \sum_{i=1}^{6} \varphi_{i,j} = 0,\ j \in \mathcal{V}_{\text{in}},$$

$$h_{\text{flatfold},j}(\boldsymbol{\varphi}) = \pi - \sum_{i=1}^{3} \varphi_{2i-1,j} = \pi - \sum_{i=1}^{3} \varphi_{2i,j} = 0,\ j \in \mathcal{V}_{\text{in}},$$

where $\varphi_{i,j}$ denotes the ith sector angle of the jth interior vertex, and $\mathcal{V}_{\text{in}}$ is the index set of all interior vertices. Moreover, the equality constraint on each sector angle $\varphi_{i,j}$ and the corresponding vertices' coordinates are considered. For example, for the kth target surface, this type of constraint for $i = 1, 2, \cdots, 6,\ j \in \mathcal{V}_{\text{in}},\ k = 1, \ldots, q$, is written as

$$\cos\varphi_{i,j} = \frac{(\mathbf{x}^k_{(i,j)} - \mathbf{x}^k_{(0,j)})^T \cdot (\mathbf{x}^k_{(i+1,j)} - \mathbf{x}^k_{(0,j)})}{\|\mathbf{x}^k_{(i,j)} - \mathbf{x}^k_{(0,j)}\| \cdot \|\mathbf{x}^k_{(i+1,j)} - \mathbf{x}^k_{(0,j)}\|}, \tag{13}$$

where $\mathbf{x}^k_{(0,j)}$ denotes the coordinates of the jth interior vertex to approximate the kth target surface.

When matching different shapes with one designed origami tessellation, all the triangles in the crease pattern are preserved, which indicates that the lengths of all creases for $j \in \mathcal{V}_{\text{in}},\ k = 1, 2, ..., q-1$ are constant during the transformation process, written as

$$h_{\text{length}}(\mathbf{x}^k, \mathbf{x}^{k+1}) = \|\mathbf{x}^k_{(0,j)} - \mathbf{x}^k_{(i,j)}\| - \|\mathbf{x}^{k+1}_{(0,j)} - \mathbf{x}^{k+1}_{(i,j)}\| = 0. \tag{14}$$

Meanwhile, for each approximate surface, the corresponding folding angles, denoted by $\boldsymbol{\theta}^k,\ k = 1, \ldots, q$, that represent the folding states, are different. These folding angles are required to satisfy the kinematics equation expressed in (8).

3) Inequality constraints: Several inequality constraints need to be considered when designing origami. Firstly, to guarantee that all creases can be easily folded, each sector angle should be placed in a specific range, i.e.,

$$g_L(\boldsymbol{\varphi}) = \varphi_{i,j} \le \varphi_{\max},\ i = 1, 2, \ldots, 6,\ j \in \mathcal{V}_{\text{in}} \tag{15a}$$

$$g_U(\boldsymbol{\varphi}) = \varphi_{i,j} \ge \varphi_{\min},\ i = 1, 2, \ldots, 6,\ j \in \mathcal{V}_{\text{in}}. \tag{15b}$$

In addition, as we mentioned above, only the vertices on one side of a partially folded origami are used to approximate a target surface. Therefore, the vertices on the other side of the origami, denoted as $\mathbf{x}(\mathbf{V}')$, should locate on one side of the target surface. Mathematically, it can be expressed as an inequality:

$$f_k(\mathbf{x}(\mathbf{V}')) \le 0,\ k = 1, \ldots, q, \tag{16}$$

where $f_k(\mathbf{x})$ is the function of the kth target surface in $\mathbb{R}^3$. These inequalities, in conjunction with the target shape's symmetric nature, restrict any deviation of these vertices from the target surface.

Combining the objective function and all constraints described above, the origami design problem is summarized as

$$\begin{aligned} \min_{\mathbf{x}^1,\ldots,\mathbf{x}^q,\boldsymbol{\varphi},\boldsymbol{\theta}^1,\ldots,\boldsymbol{\theta}^q} \quad & \max\{d_H(\mathcal{N}_{S1}, \mathcal{V}_{T1}), \ldots, d_H(\mathcal{N}_{Sq}, \mathcal{V}_{Tq})\} \\ \text{subject to } & h_{\text{develop},j}(\boldsymbol{\varphi}_j) = 0,\ j \in \mathcal{V}_{\text{in}} \\ & h_{\text{flatfold},j}(\boldsymbol{\varphi}_j) = 0,\ j \in \mathcal{V}_{\text{in}} \\ & \mathbf{T}_{\text{diff},j}(\boldsymbol{\theta}^k_j, \boldsymbol{\varphi}_j) = \mathbf{0}_3,\ j \in \mathcal{V}_{\text{in}},\ k = 1, \ldots, q. \\ & (13)\ \&\ (14)\ \&\ (15)\ \&\ (16). \end{aligned} \tag{17}$$

The developability and rigid flat-foldability constraints are linear functions on the sector angles and the folding angles. The objective function in (11) is a convex function on the coordinates of vertices. However, the kinematics constraints are nonlinear constraints. Solving the optimization problem in

(17) via an NLP solver, we can obtain the sector angles $\varphi_{i,j}$ for each interior vertex, the optimal folding angles $\boldsymbol{\theta}^k$ of creases, and the coordinates of vertices $\mathbf{x}^k$ for the kth target surface, $k = 1, \ldots, q$, from which we can calculate the edge lengths and generate the corresponding crease pattern in a paper sheet. Moreover, the 3D origami configuration can be retrieved from the vertices' coordinates, $\mathbf{x}^1, \mathbf{x}^2, \ldots, \mathbf{x}^q$.

The solution to (17) only reveals the terminal folded states of each designed origami in 3D space, whereas the transformation process is yet to be investigated. In real-world applications, the shape of the origami is the goal that really matters to the stakeholder instead of their specific locations. Therefore, in the next section, we will utilize graph rigidity theory to provide local constraints that determine the desired origami shape uniquely up to translations and rotations. With the help of these rigidity constraints, it is more flexible to search for the optimal transformation control results when guiding the transformation process. Employing rigidity constraints instead of terminal position constraints has at least three advantages: (i) the motion during the transformation process can be further constrained; (ii) the folding path and control efforts can be further optimized since the feasible set is extended; (iii) the orientation and the location of the origami at the steady state can be artificially specified by assigning partial vertices' terminal positions.

V. Rigidity-Based Triangulated Origami Shape Determination and Transformability

In this section, to achieve transformation of the origami between different shapes, a graph rigidity-based approach will be proposed to characterize the target shape of a 3D origami structure with associated folding states. We will introduce a class of frameworks, namely, triangulated frameworks, which are always contained in the crease pattern of a six-crease-based origami tessellation. Shape determination and transformability will be studied by focusing on the triangulated frameworks.

A. Introduction of Graph Rigidity Theory

In this subsection, we will briefly review the traditional graph rigidity theory [40] and propose an extended result regarding the rigidity of frameworks across different dimensional spaces. An undirected graph is denoted by $\mathcal{G} = (\mathcal{V}, \mathcal{E})$, where $\mathcal{V} = \{1, ..., n\}$ is the set of vertices, and $\mathcal{E} \subset \mathcal{V}^2$ is the set of edges. For each vertex i in $\mathcal{G}$, we assign it a position vector x_i in $\mathbb{R}^d$. The vector stacking up all vertices' positions, i.e., $\mathbf{x} = (x_1^T, ..., x_n^T)^T \in \mathbb{R}^{nd}$ is called a *configuration*. The pair $(\mathcal{G}, \mathbf{x})$ is called a *framework*. Let

$$r_{\mathcal{G}}(\mathbf{x}) = (..., ||x_i - x_j||^2, ...)^T \in \mathbb{R}^m,\ (i,j) \in \mathcal{E} \tag{18}$$

denote the *rigidity function*, where $m = |\mathcal{E}|$. The matrix

$$R_d(\mathcal{G}, \mathbf{x}) = \frac{\partial r_{\mathcal{G}}(\mathbf{x})}{\partial x} \in \mathbb{R}^{m \times nd} \tag{19}$$

is call the *rigidity matrix* in $\mathbb{R}^d$. A framework $(\mathcal{G}, \mathbf{x})$ is *infinitesimally rigid* in $\mathbb{R}^d$ if every *infinitesimal motion* $\dot{x}$ (a motion maintaining $\dot{r}_{\mathcal{G}}(\mathbf{x}) = 0$) is trivial (i.e., a translation or rotation). In other words, $\operatorname{rank}(R_d(\mathcal{G}, \mathbf{x})) = S(d) = nd - \frac{d(d+1)}{2}$, where $d(d+1)/2$ is obtained by counting d-dimensional translations and $d(d-1)/2$-dimensional rotations.

Let $\operatorname{rank}(R_d(\mathcal{G})) = \max_{\mathbf{x} \in \mathbb{R}^d} \operatorname{rank}(R_d(\mathcal{G}, \mathbf{x}))$, the following lemma shows a property of $\operatorname{rank}(R_d(\mathcal{G}))$.

Lemma V.1. *Given graph $\mathcal{G}$, the following holds:*

$$\operatorname{rank}(R_{d-1}(\mathcal{G})) \leq \operatorname{rank}(R_d(\mathcal{G})) \leq \min\{S(d), m\}. \tag{20}$$

Proof. The first inequality can be obtained by noting that a configuration x in $\mathbb{R}^{d-1}$ can always be trivially extended to a configuration in $\mathbb{R}^d$, i.e., $\mathbf{x}' = (x_1^T, 0, ..., x_n^T, 0)^T$. The second inequality is obtained by the definition of $R_d(\mathcal{G}, \mathbf{x})$. □

Another important concept we will use in this paper is *global rigidity*. A framework is globally rigid if $r_{\mathcal{G}}^{-1}(r_{\mathcal{G}}(\mathbf{x})) = r_{\mathcal{K}}^{-1}(r_{\mathcal{K}}(\mathbf{x}))$, where $\mathcal{K}$ is a complete graph.

In this paper, we will construct a new rigidity function by adding extra entries into $r_{\mathcal{G}}(\mathbf{x})$. So the concepts of infinitesimal rigidity and global rigidity will be generalized by replacing $r_{\mathcal{G}}$ in the definitions with the newly constructed rigidity function.

B. Triangulated Frameworks

Consider a triangulated framework $(\mathcal{T}, \mathbf{x})$ with $n \geq 3$ nodes, where $\mathcal{T} = (\mathcal{V}, \mathcal{E})$ is a triangulated graph defined as follows: start with a triangle composed of nodes 1, 2, and 3, at each step, add one vertex k and two edges connecting k and two vertices $i, j \in \{1, ..., k-1\}$, respectively, such that i and j are connected in the current graph. Each triangle composed of nodes i, j, k is denoted by $\Delta_{ijk} = (i, j, k)$. One can observe that the crease pattern of six-crease based origami tessellation contains a triangulated framework as a subframework. We make the following assumption for the considered triangulated framework:

Assumption 1. *Each triangle Δ_{ijk} is non-degenerate, i.e., x_i, x_j, and x_k are not collinear. Moreover, there are no overlapping vertices.*

As shown in [41], Assumption 1 implies that $(\mathcal{T}, x)$ is infinitesimally rigid in $\mathbb{R}^2$. Now we put a triangulated framework into $\mathbb{R}^3$. Then $(\mathcal{T}, \mathbf{x})$ is no longer infinitesimally rigid because $m = |\mathcal{E}| = 2n - 3 \leq 3n - 6 = S(3)$. From Lemma V.1, we have $R_2(\mathcal{T}) = R_3(\mathcal{T}) = 2n - 3 \leq S(3)$.

C. Degree-of-Freedom of Origami

For a given six-crease base, there exist $n = 7$ vertices in a unit origami. When lengths of boundary lines and creases are known and fixed, mathematically, there exist twelve equality distance constraints for the corresponding framework of this origami. Therefore, we have $\operatorname{rank}(R_2(\mathcal{T})) = 2n - 3 = 11 < 12$, which means the degree-6 vertex in a flat sheet will be infinitesimally rigid in $\mathbb{R}^2$. However, in $\mathbb{R}^3$, it is no longer infinitesimally rigid since $\operatorname{rank}(R_3(\mathcal{T})) = 12 < 15 = 3n - 6$. In other words, the DoF of a unit origami is $DoF = 3n - 6 - \operatorname{rank}(R_3(\mathcal{T})) = 3$. Then, the DoF of the six-crease origami tessellation in Fig. 2 can be calculated using the number of columns and rows. $DoF = 3n - 6 - e = 2 * col + 4 * row - 3$. Note that, based on the DoF analysis above, the minimum

number of total vertices n can be determined when designing an origami tessellation using the design framework described in Section IV. To be specific, at least n total vertices are needed, such that $DoF - 3|\mathcal{N}_S| + 6 > 0$, to approach all the discrete nodes in $\mathcal{N}_S$, which enables the origami transforming from an initially flat surface to a specified shape.

D. Local Constraints for Shape Determination

To describe the desired shape of a triangulated framework in $\mathbb{R}^3$, the edge length constraints are not enough because the DoF of the constrained shape is $3n - \text{rank}(R_3(\mathcal{T})) = n + 3$, which is greater than the dimension of trivial motion space, i.e., 6, when $n > 3$. Hence, we further introduce $n - 3$ angle constraints into the rigidity function $r_{\mathcal{T}}(\mathbf{x})$, so that $\text{rank}(\frac{\partial r_{\mathcal{T}}(\mathbf{x})}{\partial \mathbf{x}})$ reaches its maximum value, i.e., $3n - 6$ in $\mathbb{R}^3$, which renders the DoF of the formation minimum. Note that a constraint on the angle between two edges (i, j) and (i, k) is equivalent to a constraint on the inner product $(x_i - x_j)^T(x_i - x_k)$ if both $||x_i - x_j||$ and $||x_i - x_k||$ are fixed. Hence, similar to [42], we have constraint on $(x_i - x_j)^T(x_i - x_k)$ directly.

Next we explain which angle we want to constrain. For each vertex $k > 3$, we can specify an edge (i_k, j_k) based on which k is inserted, i.e., $(i_k, j_k) \in \Delta$ and $i_k < j_k < k$. Then we find another vertex l such that $(l_k, i_k, j_k) \in \Delta$ and $l_k < k$. Note that l_k must exist because the framework is triangulated before vertex k is inserted. Then we can determine a quaternion corresponding to two triangles with one common edge for each $k > 3$, and we denote it by $Q(k) = \{l_k, i_k, j_k, k\}$. Note that here i_k and j_k are uniquely determined, but there may be multiple choices for l_k such that $(l_k, i_k, j_k) \in \Delta$. In our work, without loss of generality[1], we choose $l_k = \min\{l \in \mathcal{V} : (l, i_k, j_k) \in \Delta\}$. Then $Q(k)$ is uniquely determined for each vertex $k > 3$. As a result, we can uniquely determine a function $A(k) = (j_k, l_k, k)$. Now we are able to specify the angles we want to constrain. Define the *angle index set* as $\mathcal{A} = \{A(k) : k = 4, ..., n\}$. It can be observed that $|\mathcal{A}| = n - 3$. Figure 7 (a) shows a non-degenerate triangulated framework. In this example, we have $Q(4) = \{1, 2, 3, 4\}$, $Q(5) = \{3, 2, 4, 5\}$, $\mathcal{A} = \{(3, 1, 4), (4, 3, 5)\}$.

Accordingly, we define a new rigidity function containing the inner products corresponding to all the angles under constraints, written as

$$r_A(\mathbf{x}) = (..., (x_i - x_j)^T(x_i - x_k), ...)^T, \ (i, j, k) \in \mathcal{A}. \quad (21)$$

Let $r(\mathbf{x}) = (r_{\mathcal{T}}^T(\mathbf{x}), r_A^T(\mathbf{x}))^T$ be the new rigidity function containing both distance and angle, and $R(\mathbf{x}) = \frac{\partial r(\mathbf{x})}{\partial \mathbf{x}}$ be the new rigidity matrix. Let $\mathcal{P} = \{k \in \{4, ..., n\} : x_{l_k}, x_{i_k}, x_{j_k}, x_k \text{ are coplanar}\}$ be the set of vertices k corresponding to which the two triangles determined by $Q(k)$ are coplanar. Then we have the following lemma.

Lemma V.2. *Under Assumption 1,* $\text{rank}(R(\mathbf{x})) = 3n - 6 - |\mathcal{P}|$.

Proof. Based on $r_A(\mathbf{x})$, we construct another rigidity function

$$r_D(\mathbf{x}) = (..., ||x_j - x_k||^2, ...)^T, \ (i, j, k) \in \mathcal{A}. \quad (22)$$

[1]In practice, l_k can be chosen as any $l < k$ such that $(l, i_k, j_k) \in \Delta$.

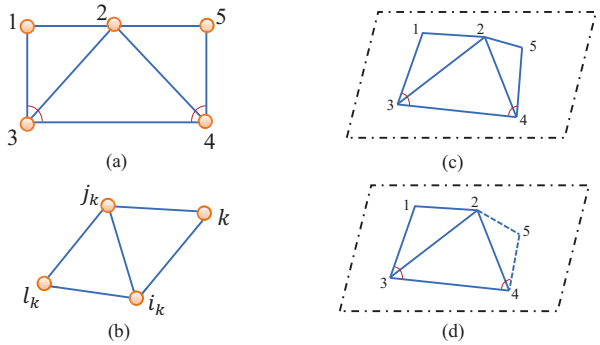

Fig. 7: (a) A triangulated framework with 5 vertices in $\mathbb{R}^2$, (b) An illustration for Q_k, (c) and (d) are two possible realizations in $\mathbb{R}^3$ given distance constraints and two angle constraints. In (c), both vertices 1 and 5 are above the plane. In (d), vertex 1 is located above the plane, while vertex 5 is below the plane [38]

.

Let $r'(\mathbf{x}) = (r_{\mathcal{T}}^T(\mathbf{x}), r_D^T(\mathbf{x}))^T$ and $R'(\mathbf{x}) = \frac{\partial r'(\mathbf{x})}{\partial \mathbf{x}}$. Note that for any $(i, j, k) \in \mathcal{A}$, we have $(i, j), (i, k) \in \mathcal{E}$. Moreover, for any $i, j, k \in \mathcal{V}$, it holds that

$$||x_j - x_k||^2 = ||x_i - x_j||^2 + ||x_i - x_k||^2 - 2(x_i - x_j)^T(x_i - x_k).$$

This implies that $r(\mathbf{x}) = (r_{\mathcal{T}}^T(\mathbf{x}), r_A^T(\mathbf{x}))^T$ and $r'(\mathbf{x})$ can be linearly denoted by each other. As a result, $\text{rank}(R'(\mathbf{x})) = \text{rank}(R(\mathbf{x}))$. Next we show $\text{rank}(R'(\mathbf{x})) = 3n - 6 - |\mathcal{P}|$.

For $n = 3$, under Assumption 1, $\text{rank}(R'(\mathbf{x})) = \text{rank}(R(\mathbf{x})) = \text{rank}(R(\mathcal{T}, \mathbf{x})) = 3 = 3 \times 3 - 6 - 0$.

For $n = k - 1$, $x \in \mathbb{R}^{3(k-1)}$, we add one vertex x_k, and two edges (k, i_k) and (k, j_k) into the framework. Let $x' = (x^T, x_k^T)^T \in \mathbb{R}^{3k}$, there must exist l_k such that l_k is connected to i_k and j_k, and $r'(\mathbf{x}') = (r'^T(\mathbf{x}), ||e_{ki_k}||^2, ||e_{kj_k}||^2, ||e_{kl_k}||^2)^T$, where $e_{ks} = x_k - x_s$. Then $\text{rank}(R'(\mathbf{x}')) = \begin{pmatrix} \frac{\partial r'(\mathbf{x})}{\partial \mathbf{x}} & \mathbf{0}_{(3(k-1)-6)\times 3} \\ S_1 & S_2 \end{pmatrix}$, where $S_2 = (e_{ki_k}, e_{kj_k}, e_{kl_k})^T$. Note that Under Assumption 1, $\text{rank}(S_2) = 2$ if $k \in \mathcal{P}$ and $\text{rank}(S_2) = 3$ otherwise. Together with $\text{rank}(R'(\mathbf{x}')) = \text{rank}(R'(\mathbf{x})) + \text{rank}(S_2)$, we have $\text{rank}(R(\mathbf{x})) = 3n - 6 - |\mathcal{P}|$ for a general n. □

In fact, even when $|\mathcal{P}| = 0$, $r(\mathbf{x})$ is still not able to uniquely determine the formation shape, because an infinitesimally rigid framework may not be globally rigid. For example, in Fig. 7 (a), there are $n = 5$ agents, $2n - 3 = 7$ edge length constraints, and $n - 3 = 2$ angle constraints. Although $\text{rank}(R(\mathbf{x})) = \text{rank}(\frac{\partial r(\mathbf{x})}{\partial \mathbf{x}}) = 3n - 6 = 9$, there are two possible shapes shown in (c) and (d). On the other hand, global rigidity does not imply infinitesimal rigidity. A simple example for this fact is a framework $(\mathcal{K}, \mathbf{x})$ with configuration $\mathbf{x}$ being degenerate.

In order to uniquely determine the origami shape in $\mathbb{R}^3$, we aim to design a rigidity function such that the framework is globally rigid. To this end, we further add $n - 3$ sign constraints, which determine the relative position between any two triangles with a common edge. Such an addition is to further reduce the DOF of the current distance-constrained

framework, so that all the infinitesimal motions become trivial. For each $k = 4, ..., n$, we define

$$\sigma_k(\mathbf{x}) = \text{sign}(\begin{vmatrix} x_k - x_{i_k} & x_{j_k} - x_{i_k} & x_{l_k} - x_{i_k} \end{vmatrix}), \quad (23)$$

which determines which side of the plane (denoted by $\Delta_{l_k i_k j_k}$) vertex k is located in. σ_k is actually determined by the sign of the cosine value of the angle between $x_k - x_{i_k}$ and the normal vector of the $\Delta_{l_k i_k j_k}$ plane.

We define the shape formed by a configuration x as follows:

$$\mathscr{S}_x = \{y \in \mathbb{R}^{3n} : y = (I_n \otimes R)x + \mathbf{1}_n \otimes \xi, R \in \text{SO}(3), \xi \in \mathbb{R}^3\}.$$

Here $\mathscr{S}_x \subsetneqq r_{\mathcal{K}}^{-1}(r_{\mathcal{K}}(\mathbf{x}))$ if $\mathbf{x}$ is non-degenerate because $r_{\mathcal{K}}^{-1}(r_{\mathcal{K}}(\mathbf{x}))$ contains reflections of the configuration $\mathbf{x}$, while $\mathscr{S}_x$ does not.

The following theorem shows that regardless of $|\mathcal{P}|$, the rigidity function $r(\mathbf{x})$, together with $\sigma_k(\mathbf{x})$, $k = 4, ..., n$, determine the formation shape uniquely.

Theorem V.1. *Under Assumption 1, the rigidity function $r(\mathbf{x})$, together with $\{\sigma_k(\mathbf{x}), k = 4, ..., n\}$ determine the shape of $(\mathcal{T}, \mathbf{x})$ uniquely. That is,*

$$r^{-1}(r(\mathbf{x})) \cap (\cap_{k=4}^{n} \sigma_k^{-1}(\sigma_k(\mathbf{x}))) = \mathscr{S}_x. \quad (24)$$

Proof. Let $U = r^{-1}(r(x)) \cap (\cap_{k=4}^{n} \sigma_k^{-1}(\sigma_k(\mathbf{x})))$. Note that it must hold $U \supseteq \mathscr{S}_x$ because $r(\mathbf{x})$ and $\sigma_k(\mathbf{x})$ are invariant under rotations and translations. Next, we prove $U \subseteq \mathscr{S}_x$ by induction.

For $n = 3$, since the reflection of a triangle in $\mathbb{R}^3$ can be achieved by rotations, we have $\mathscr{S}_x = r_{\mathcal{K}}^{-1}(r_{\mathcal{K}}(\mathbf{x}))$. Hence, the statement is true.

Suppose that $U \subseteq \mathscr{S}_x$ holds for $n = k - 1 \geq 3$. Now we add vertex k and edges (k, i_k) and (k, j_k). As explained in the first paragraph of the proof of Lemma V.2, if $r(\mathbf{x})$ is known, $r'(\mathbf{x})$ is known as well. Hence, it suffices to show that given $x \in \mathbb{R}^{3(k-1)}$, the location of the newly added vertex k can be uniquely determined by $r'(\mathbf{x})$ and σ_k. Note that $r'(\mathbf{x})$ contains the distance between any two pairs of vertices in $Q(k)$. That is, we have a distance rigidity function $r_{\mathcal{K}(k)}$ (which is a subvector of $r'(\mathbf{x})$) corresponding to a complete graph with vertices in $Q(k)$.

If $k \in \mathcal{P}$, then $\sigma_k = 0$, x_k can be uniquely determined in the plane determined by vertices l_k, i_k and j_k, because Assumption 1 implies that any two of edges (k, l_k), (k, j_k) and (k, l_k) cannot be collinear. If $k \notin \mathcal{P}$, the vertices in $Q(k)$ form a tetrahedron in $\mathbb{R}^3$. Although a tetrahedron is globally rigid, there are two possible positions for k on the two different sides of the plane determined by vertices l_k, i_k, and j_k, because global rigidity allows reflections. With $\sigma_k(\mathbf{x})$ at hand, x_k is uniquely determined. □

E. Transformability

In this subsection, we will show the feasibility of the transformation between two shapes while preserving the physical edge length of the origami.

Let $\mathbf{x}(t)$ be the configuration, i.e., the vector composed of vertex positions of the origami at time t. Define a set $\mathcal{X}_{\mathcal{T}}(\mathbf{x}(0)) = \{\mathbf{x} \in \mathbb{R}^{3n} : r_{\mathcal{T}}(\mathbf{x}) = r_{\mathcal{T}}(\mathbf{x}(0))\} = r_{\mathcal{T}}^{-1}(r_{\mathcal{T}}(\mathbf{x}(0)))$. The following lemma shows that $\mathbf{x}(0)$ can be continuously transformed to $\mathbf{x}(t)$ within $\mathcal{X}_{\mathcal{T}}(\mathbf{x}(0))$ for any $\mathbf{x}(t) \in \mathcal{X}_{\mathcal{T}}(\mathbf{x}(0))$.

Lemma V.3. *(Transformability) There exists a continuous path in $\mathcal{X}_{\mathcal{T}}(\mathbf{x}(0))$ between any two distinct configurations $\mathbf{x}(0), \mathbf{x}(t) \in \mathcal{X}_{\mathcal{T}}(\mathbf{x}(0))$.*

Proof. Given two distinct configurations $\mathbf{x}(0), \mathbf{x}(t) \in \mathcal{X}_{\mathcal{T}}(\mathbf{x}(0))$. We consider two cases as follows.

Case 1. $\mathbf{x}(t) \in r_{\mathcal{K}}^{-1}(r_{\mathcal{K}}(\mathbf{x}(0)))$. Then $\mathbf{x}(t)$ can be transformed from $\mathbf{x}(0)$ by continuous uniform rotations and translations of the whole configuration.

Case 2. $\mathbf{x}(t) \in \mathcal{X}_{\mathcal{T}}(\mathbf{x}(0)) \setminus r_{\mathcal{K}}^{-1}(r_{\mathcal{K}}(\mathbf{x}(0)))$. Note that $(\mathcal{T}, \mathbf{x})$ is not rigid. According to [40, Proposition 1], $(\mathcal{T}, \mathbf{x})$ is flexible. That is, there exists a continuous path from $\mathbf{x}$ to any $\mathbf{x}(t) \in \mathcal{X}_{\mathcal{T}}(\mathbf{x}(0)) \setminus r_{\mathcal{K}}^{-1}(r_{\mathcal{K}}(\mathbf{x}))$. □

VI. Optimal Transformation Control

For the designed origami tessellation, each target 3D surface has associated folding angles, which indicates that by controlling the folding angles during the transformation process, the tessellation will transform into the desired 3D shape. However, there may exist many feasible folding paths that guide the origami from an initial crease pattern to a 3D target shape. To reduce the control efforts during the transformation process while guaranteeing controllability, the origami folding motion control problem is formulated as a constrained optimal control problem to minimize the control efforts subject to system dynamics, local shape-preserving constraints, and initial and terminal boundary conditions.

A. Transformation Control with Triangulated Constraints

Consider a multi-agent system with $n \geq 4$ agents, each agent has the following dynamics,

$$\dot{x}_i(t) = f_i(x_i, u_i, t), \quad (25)$$

where $x_i(t) \in \mathbb{R}^3$ and $u_i(t) \in \mathbb{R}^3$ denote the position state vector and control input vector of agent i at time t, respectively. By modeling each agent i as a vertex of the framework $(\mathcal{G}, \mathbf{x})$, the 3D shape of an origami can be described by a rigid framework, where each edge of $\mathcal{G}$ represents a distance constraint. Moreover, each agent with $\dot{x}_i(t) = f_i(x_i, u_i, t)$ is assumed to be controllable.

We first consider a triangulated configuration $(\mathcal{T}, \mathbf{x})$ in $\mathbb{R}^2$ as the initial states of the origami in a 2D plane. Then the transformation control problem in this paper is to drive a multi-agent system from a triangulated configuration continuously from $\mathbb{R}^2$ to a desired shape in $\mathbb{R}^3$ while maintaining the local shape of each cluster of agents by preserving the distance of each pair of adjacent agents. By denoting $\mathbf{x}(t) = (x_1^T(t), ..., x_n^T(t))^T$, and $u(t) = (u_1^T(t), ..., u_n^T(t))^T$, the transformation control problem is stated as follows.

Problem 1. *Given two frameworks $(\mathcal{T}, \mathbf{x}^*)$ with $\mathbf{x}^* \in \mathcal{X}_{\mathcal{T}}(\mathbf{x}(0))$ and $(\mathcal{T}, \mathbf{x}(0))$ describing the desired shape and the initial shape of a multi-agent system, respectively. Find a control strategy $u(t)$, $t \in [0, t_f]$ such that the multi-agent system (25) achieves a target shape with the same shape as*

that of $(\mathcal{T}, \mathbf{x}^*)$ *at time* $t = t_f$*, while maintaining the distance constraints in* $(\mathcal{T}, \mathbf{x}(0))$.

In this paper, we say two frameworks $(\mathcal{G}, \mathbf{x})$ and $(\mathcal{G}, \mathbf{y})$ have the same shape if $\mathbf{x}$ can be transformed from $\mathbf{y}$ by translations and rotations. The feasibility of Problem 1 is guaranteed by combining the transformability of $(\mathcal{T}, \mathbf{x}^*)$ and the controllability of dynamic vertices. Specifically, the transformability condition ensures that there exists a continuous path between the initial shape and the desired shape, which is proven in Lemma V.3. In addition, each agent in the system is supposed to be controllable.

B. Optimal Transformation Control with Constant Constraints

Problem 1 is to search for a feasible control maneuver to reach the target shape while satisfying local shape constraints. However, there may exist many feasible control strategies to steer all agents to the target formation. Among all the feasible solutions, our goal is to find the optimal control maneuver to drive the system from the initial 2D configuration to the target 3D shape with minimum control efforts. Accordingly, this optimal control problem can be formally stated as follow.

Problem 2. *Find a control strategy* $u(t)$*,* $t \in [0, t_f]$ *to minimize the control efforts* $\int_0^{t_f} ||\mathbf{u}(t)||dt$ *of the multi-agent system (25) in solving Problem 1.*

Mathematically, Problem 2 can be formulated as

$$\begin{aligned} \min_{\mathbf{u}}(t) & \int_0^{t_f} ||\mathbf{u}(t)||dt \qquad (26)\\ \text{s.t.} \quad & \dot{\mathbf{x}}(t) = f(\mathbf{x}, \mathbf{u}, t), \quad t \in [0, t_f],\\ & r_{\mathcal{T}}(\mathbf{x}(t)) = r_{\mathcal{T}}(\mathbf{x}(0)), \quad t \in [0, t_f],\\ & r_A(\mathbf{x}(t_f)) = r_A(\mathbf{x}^*),\\ & \sigma_k(\mathbf{x}(t_f)) = \sigma_k(\mathbf{x}^*),\ k = 4, ..., n \end{aligned}$$

where $r_{\mathcal{T}}(\mathbf{x}(0))$ defines the initial configuration in $\mathbb{R}^2$, $\mathcal{T}(\mathbf{x}(0))$, together with $r_A(\mathbf{x}^*)$ and $\sigma_k(\mathbf{x}^*)$ determinate the target formation uniquely in $\mathbb{R}^3$, and t_f is given. Similar to Problem 1, Problem 2 is feasible due to the transformability of the triangulated origami and the controllability of agents (25).

Remark 1. *According to Theorem V.1, the origami shape in* $\mathbb{R}^3$ *can be uniquely determined by assigning the rigidity function* $r(\mathbf{x})$ *associated with* $\sigma_k(\mathbf{x})$*. Specifically, during the origami folding motion, the lengths of all edges are constant, which are constrained in* $r_{\mathcal{T}}(\mathbf{x}(t)) = r_{\mathcal{T}}(\mathbf{x}(0)), \quad t \in [0, t_f]$*. Meanwhile,* $r_A(\mathbf{x}(t_f)) = r_A(\mathbf{x}^*)$ *and* $\sigma_k(\mathbf{x}(t_f)) = \sigma_k(\mathbf{x}^*)$ *constrain* $n - 3$ *terminal folding angles of origami creases. Thus, once the origami shape is designed from* (17)*, the corresponding rigidity function* $r(\mathbf{x})$ *and sign function* $\sigma_k(\mathbf{x})$ *can be obtained, and then the folding trajectories will be determined from the flat sheet to the desired 3D origami shape. The initial state* $\mathbf{x}(0)$ *corresponds to either a 2D shape or a 3D shape, but the terminal state always determines a 3D shape. As a result, Problem 2 can represent the transformation process of an origami from a 2D shape to a 3D shape or between two 3D shapes.*

Based on the definitions of rigidity function for distance-based and angle-based constraints in (18) and (21), both $r_{\mathcal{T}}$ and r_A are quadratic equality constraints on state variables $\mathbf{x}$. In addition, σ is a binary variable with a nonlinear constraint on $\mathbf{x}$. Therefore, (26) is classified as a nonlinear optimal control problem. The existence of constant constraints on the local shape of configuration restricts the freedom of transition and makes the transformation control more challenging. By discretizing all agents' trajectories from initial time t_0 to terminal time t_f into a group of discrete nodes represented by states and control variables at each node, Problem 2 is transformed into an NLP problem via collocation method and solved using a sparse sequential quadratic programming (SQP) algorithm [43] embedded in Tomlab/SNOPT solver [44].

VII. Simulation Example

In this section, we will present an example to illustrate the origami design framework for approximating two different 3D surfaces, and then simulate the folding process of the designed origami using the optimal transformation control strategy discussed in Section VI. All the simulations are executed in Matlab environment on a laptop with Intel(R) Core(TM) i7-6700 (8 cores, 3.41Gz).

A. Target 3D Surfaces and Discretization

In this example, we consider two target surfaces in Fig. 8. One is an elliptical surface, and the other one is a hyperbolic surface. The expressions of these two target surfaces can be written as

$$\frac{x^2}{a^2} + \frac{y^2}{b^2} + \frac{z^2}{c^2} = 1, \qquad (27a)$$

$$\frac{x^2}{a^2} + \frac{y^2}{b^2} - \frac{z^2}{c^2} = 1, \qquad (27b)$$

where $a = \sqrt{2}/2, b = \sqrt{2}/2, c = 1$ are the constant coefficients. Obviously, both of these two target surfaces are rotationally symmetric and can be discretized into N equal sections, respectively. Here, N denotes the order of rotational symmetry and is set as 12 in this example. For every $1/N$ part, 9 discrete nodes are selected to represent the section of each target surface. In addition, the two target surfaces are also symmetric about the $x - y$ plane. Therefore, only half of these nine nodes are needed to represent these two surfaces. The intersections are denoted as $\mathcal{N}_{S1} = \{\mathbf{p}_1^1, \mathbf{p}_2^1, \cdots, \mathbf{p}_5^1\}$ and $\mathcal{N}_{S2} = \{\mathbf{p}_1^2, \mathbf{p}_2^2, \cdots, \mathbf{p}_5^2\}$. Specifically, the coordinates of the five nodes are listed in Table. I.

TABLE I: Discrete nodes on the two target surfaces.

$\mathcal{N}_{S1}$		$\mathcal{N}_{S2}$	
$\mathbf{p}_1^1$	$[0, -0.354, 0.87]^T$	$\mathbf{p}_1^2$	$[0; -1; 1]^T$
$\mathbf{p}_2^1$	$[0, -0.612, 0.5]^T$	$\mathbf{p}_2^2$	$[0; -0.819; 0.583]^T$
$\mathbf{p}_3^1$	$[-0.179, -0.660, 0.259]^T$	$\mathbf{p}_3^2$	$[-0.189; -0.704; 0.259]^T$
$\mathbf{p}_4^1$	$[0.179, -0.660, 0.259]^T$	$\mathbf{p}_4^2$	$[0.189; -0.704; 0.259]^T$
$\mathbf{p}_5^1$	$[0, -0.707, 0]^T$	$\mathbf{p}_5^2$	$[0; -0.707; 0]^T$

To approximate the five discrete nodes, $\mathbf{p}_1^k, \cdots, \mathbf{p}_5^k$, $k = 1, 2$ of the $1/N$ part section, five interior vertices of the origami

to be designed are used. Thus, $DoF-(3|\mathcal{N}_S|-6)=2\geq 1$. Let $\mathbf{v}_i$, $i=1,2,3,...,19$, denote the vertices of the crease pattern and $\mathbf{x}_i^1$, $\mathbf{x}_i^2$ be the corresponding points in the 3D space for approximating the two target surfaces, respectively. Note that, each unit origami in a tessellation has seven vertices, but at most three of them can be assigned to approach the discrete nodes, such that the DoF of each unit origami will be larger than 1. Specifically, in this case, $\mathcal{V}_{T1}$ and $\mathcal{V}_{T2}$ are selected as $\{\mathbf{x}_1^1,\mathbf{x}_7^1,\mathbf{x}_{11}^1,\mathbf{x}_{12}^1,\mathbf{x}_{16}^1\}$ and $\{\mathbf{x}_1^2,\mathbf{x}_7^2,\mathbf{x}_{11}^2,\mathbf{x}_{12}^2,\mathbf{x}_{16}^2\}$ to approximate the $1/N$ part of two target surfaces, respectively.

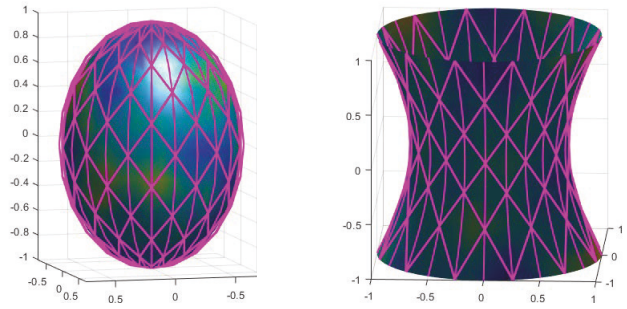

(a) (b)

Fig. 8: Discretization of two target surfaces: (a) Hyperbolic surface; (b) Elliptical surface.

B. Optimal Design Results of Origami Tessellation

After discretizaiton of target surfaces, the optimization problem in (17) can be organized via combining all equality and inequality constraints. The design variables are collected as $\mathbf{x}=[\mathbf{x}_1^1,\cdots,\mathbf{x}_{19}^1,\mathbf{x}_1^2,\cdots,\mathbf{x}_{19}^2,\varphi_{(1,1)},\cdots,\varphi_{(1,6)},\varphi_{(2,1)},\cdots,\varphi_{(5,6)},\theta_{4,1}^1,\cdots,\theta_{i,j}^1,\cdots,\theta_{16,6}^1,\theta_{4,1}^2,\cdots,\theta_{i,j}^2,\cdots,\theta_{16,6}^2]^T$. where $i=4,7,10,13,16$ and $j=1,\cdots,6$. In addition, let $w_1=w_2=w_3=w_4=1,w_5=100$, $\varphi_{\min}=20^\circ,\varphi_{\max}=140^\circ$, and

$$f_1(\mathbf{x}_{\mathcal{V}_{T1}})=\frac{x^2}{a^2}+\frac{y^2}{b^2}+\frac{z^2}{c^2}-1\leq 0,$$
$$f_2(\mathbf{x}_{\mathcal{V}_{T2}})=\frac{x^2}{a^2}+\frac{y^2}{b^2}-\frac{z^2}{c^2}-1\leq 0.$$

Solving the resulting optimization problem via an NLP solver (e.g., the interior point method of '$fmincon$' in Matlab), we can obtain the optimal design results of the half of $1/N$ part crease pattern. After the half $1/N$ part of the crease pattern is determined, the other $1/N$ part crease pattern can be obtained by creating its symmetric part about the x-y plane, as shown in Fig. 9 (a) and (b). The developability and flat-foldability at the interior vertices are guaranteed when NLP obtains a converged result.

In addition, for the designed $1/N$ origami shown in Fig. 9 (c) and (d), the folding angles at the desired states can be obtained from the solution to problem (17), which are listed in Table II, where $\theta_{i,:}, i=4,7,10,13,16$, denote the folding angles along the six creases for the ith interior vertex. Note that, due to geometry continuity, we have $\theta_{7,1}=\theta_{4,4}$, $\theta_{10,1}=\theta_{7,4}$, $\theta_{13,1}=\theta_{10,4}$ and $\theta_{16,1}=\theta_{13,4}$.

TABLE II: Folding angles of creases for two designed origami structures.

	$\boldsymbol{\theta}_{S1}^*$ /rad
$\theta_{4,:}^1$	$[0.38,-0.97,0.16,-0.52,0.16,-0.97]^T$
$\theta_{7,:}^1$	$[-0.52,0.042,-0.012,-0.51,0.033,-0.019]^T$
$\theta_{10,:}^1$	$[-0.51,0.14,-1.38,0.39,-1.38,0.14]^T$
$\theta_{13,:}^1$	$[0.39,-1.44,-0.13,0.88,-0.13,-1.44]^T$
$\theta_{16,:}^1$	$[0.88,-1.16,-1.14,0.86,-1.14,-1.16,0.88]^T$
	$\boldsymbol{\theta}_{S2}^*$ /rad
$\theta_{4,:}^2$	$[-0.17,-0.98,0.55,-0.93,0.55,-0.98]^T$
$\theta_{7,:}^2$	$[-0.93,1.37,0.24,0.52,0.24,1.37]^T$
$\theta_{10,:}^2$	$[0.52,-0.23,-0.30,0.32,-0.30,-0.23]^T$
$\theta_{13,:}^2$	$[0.32,-0.48,-0.24,-0.17,-0.24,-0.48]^T$
$\theta_{16,:}^2$	$[-0.17,0.24,0.24,-0.17,0.24,0.24]^T$

Furthermore, the position vectors $\mathbf{x}^1$ and $\mathbf{x}^2$ of each vertex are obtained from the design results, which is then used to shape the folded origami for approximating the two target surfaces, shown in Figs. 9 (c)-(d). The entire crease pattern can be generated by periodically repeating the $1/N$ part N times. Moreover, according to the signs and values of folding angles, the MV assignments for the two surfaces are demonstrated in Figs. 10 (a) and (c), where the blue and red lines denote the mountain and valley folding, respectively, and the transparency of creases are determined by the ratio $\varphi_{i,j}/\pi$. The tessellation designs in Figs. 10 (a) and (c) are the same. The only difference is the MV assignments for the two surfaces. The corresponding 3D structures of the optimally designed origami are shown in Figs. 10 (b) and (d), where the dash lines represent the target surfaces. The designed results verify that the two target shapes are approximated by the 3D origami structures. Although the vertices $\mathcal{V}_{T1}$ and $\mathcal{V}_{T2}$ are not exactly coincided with intersections in $\mathcal{N}_{T1}$ and $\mathcal{N}_{T2}$, the summation of distances between assigned vertices and target points, denoted by $\sum_{i=1}^{|\mathcal{N}_S|}\|\mathbf{p}_i-\mathbf{x}_i(\mathcal{V}_T)\|$, are 0.905 and 1.427 for the two 3D surfaces, respectively, which are relatively small. The result indicates that with the limited DoF, the two desired shapes are closely approximated. The design results verify the effectiveness of the proposed framework for designing a crease pattern to approximate multiple 3D surfaces.

C. Transformation Control of Origami Folding Process

In this section, we demonstrate that the formulation of the optimal control problem in (26) is efficient to guide the origami designed in Fig. 10 from a 2D flat surface to a 3D target shape. Due to the rotational symmetric structures of the designed 3D origami, only half of $1/N$ parts will be considered here. Each agent/vertex of the origami is characterized with single integrator dynamics of the form $\dot{x}_i(t)=u_i(t)$. As a result, minimizing the objective function is to find the shortest path from the initial configuration in Fig. 10 (a) and (c) to the corresponding target 3D surface in Fig. 10 (b) and (d). Moreover, based on the analysis in Section V, $n-3=16$ folding angles and the corresponding sign function $\sigma_k(\mathbf{x})$ are needed to uniquely determine the origami shape in $\mathbb{R}^3$, where

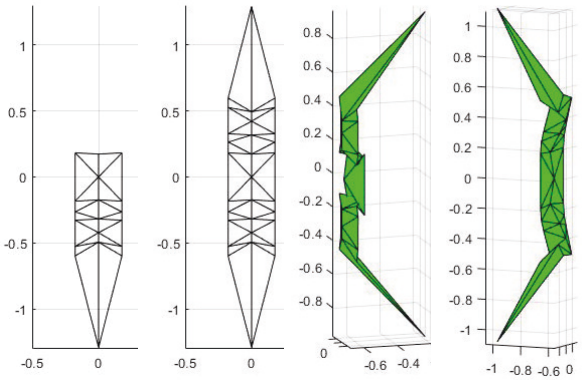

(a) (b) (c) (d)

Fig. 9: Optimal design of origami: (a) Half of $1/N$ part; (b) $1/N$ part by reflection; (c) the optimal folded status for $1/N$ elliptical surface; (d) the optimal folded status for $1/N$ hyperbolic surface.

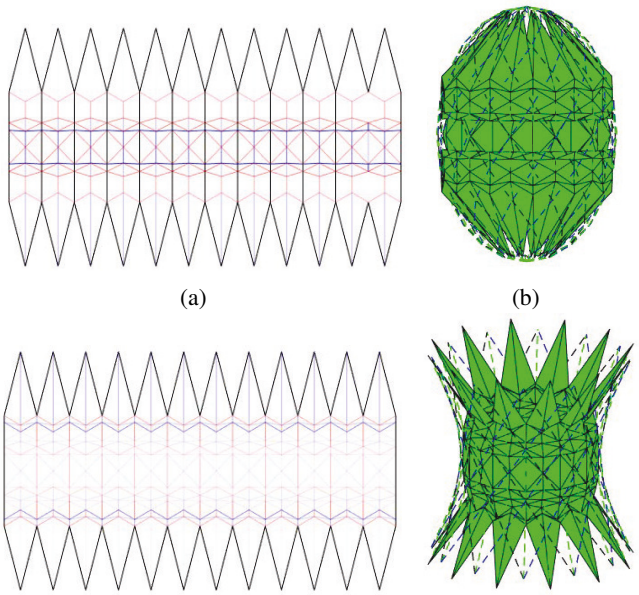

(a) (b) (c) (d)

Fig. 10: The optimized crease-pattern: (a) MV assignment of the elliptical surface; (b) 3D elliptical surface; (c) MV assignment of the hyperbolic surface; (d) The 3D hyperbolic surface.

$n = 19$ is the total number of vertices in the $1/N$ part of origami tessellation. From the kinematic equation in (8), we know that at most three of the six folding angles for each unit origami are independent. Then, without loss of generality, in this case, $\theta_{4,1:3}, \theta_{7,2:4}, \theta_{10,2:4}, \theta_{13,2:4}$ and $\theta_{16,2:5}$ in Table II are selected as the boundary conditions for the formation control problem, i.e., $r_A(\mathbf{x}^*)$ and $\sigma_k(\mathbf{x}^*)$ in Problem (26) to uniquely determine the terminal 3D shape of origami.

Solving the resulting optimal control problems in (26) will guide the designed origami to realize the folding status of the two approximated shapes with corresponding folding angles, respectively. The optimal control results in Figs. 11 (a)-(b) demonstrate the minimum-cost paths for all agents in both cases, where the blue dash lines represent the initial 2D crease pattern, the black solid lines stand for the 3D structures, and the red curves are the optimal trajectories. The optimal control efforts $\int_0^{t_f} \|u(t)\| dt$ for the solutions in Figs. 11 (a) and (b) are 15.07 and 7.11, respectively. Additionally, to demonstrate the significant reduction in the control efforts using the optimal control approach, we solve the corresponding feasibility problems by setting the objective as 0 for Problem 2. The corresponding control efforts from the feasibility solutions are 69.65 and 34.41, respectively, which are much higher than the optimal control efforts. The corresponding trajectories from the feasible solutions are shown in Figs. 11 (c) and (d).

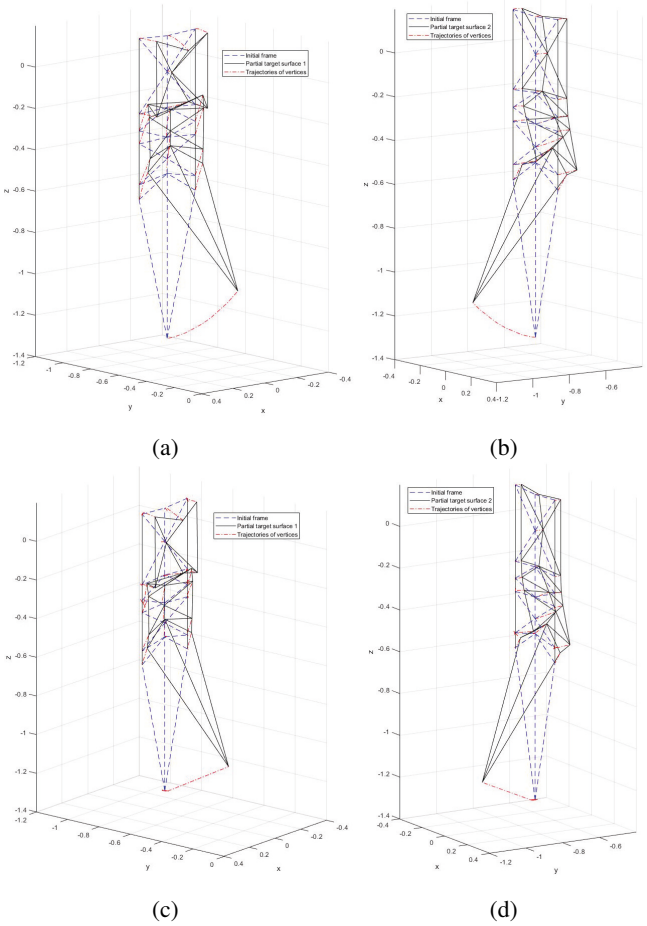

(a) (b) (c) (d)

Fig. 11: Optimal and feasible trajectories of each vertex from 2D crease pattern to 3D origami structures: (a) optimal trajectories to elliptical surface; (b) optimal trajectories to hyperbolic surface; (c) feasible trajectories to elliptical surface; (d) feasible trajectories to hyperbolic surface.

Furthermore, to validate the triangular shape-preserving during the folding process in the formation maneuver, we define the maximum error of the distance constraints as

$$\Delta E_i(t) = \{|e_i(t) - e_{i,0}|, i \in \mathcal{E}\} \tag{28}$$

where $e_{i,0}$ denotes the lengths of edges in the crease pattern. In the problem, there are forty distance constraints to be preserved. Figures 12 (a)-(b) present the time histories of

mean value and deviation of $\Delta e_i(t)$ during the folding process to the two 3D approximate shapes, respectively. Obviously, during the maneuver process, the maximum errors of the distance constraints for the two target shapes are smaller than $4e-13$ and $6e-13$, which are sufficiently close to zero. The simulation results verify that the triangular shape-preserving constraints are satisfied during the folding process.

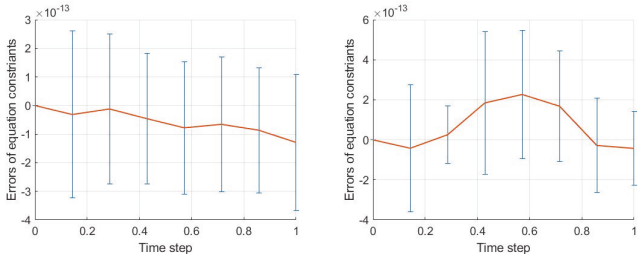

(a) (b)

Fig. 12: Maximum errors $\Delta e_{\max}(t)$ of distance constraints during the folding process: (a) for the elliptical surface; (b) for the hyperbolic surface.

VIII. Conclusion

This paper develops a systematic approach to origami tessellation design for approximating 3D surfaces, and the transformation process control of the origami. The design framework can find an origami tessellation with associated folding status to match each target surface as close as possible. By introducing a rigidity function combining distance constraints and angle constraints, a target shape can be uniquely determined up to translations and rotations. Then the transformation process between two target shapes is formulated as an optimal control problem subject to system dynamics and local shape preservation constraints. An example of designing an origami tessellation and controlling its transformation process to approximate both elliptical and hyperbolic surfaces is presented, which verifies the effectiveness of the design framework and the optimal transformation control strategy. In our future work, we will extend our transformation control approach to a distributed control framework to further improve control efficiency.

References

[1] T. Hull, "On the mathematics of flat origamis," *Congressus numerantium*, pp. 215–224, 1994.
[2] T. Tachi, "Generalization of rigid-foldable quadrilateral-mesh origami," *Journal of the International Association for Shell and Spatial Structures*, vol. 50, no. 3, pp. 173–179, 2009.
[3] D. Dureisseix, "An overview of mechanisms and patterns with origami," *International Journal of Space Structures*, vol. 27, no. 1, pp. 1–14, 2012.
[4] C. C. Chu and C. K. Keong, "The review on tessellation origami inspired folded structure," in *AIP Conference Proceedings*, vol. 1892, no. 1, 2017, p. 020025.
[5] A. R. Ahmed, O. C. Gauntlett, and G. Camci-Unal, "Origami-inspired approaches for biomedical applications," *ACS omega*, vol. 6, no. 1, pp. 46–54, 2020.
[6] S. Debnath and L. Fei, "Origami theory and its applications: a literature review," *World Academy of Science, Engineering and Technology*, pp. 1131–1135, 2013.
[7] Y. Nishiyama, "Miura folding: Applying origami to space exploration," *International journal of pure and applied mathematics*, vol. 79, no. 2, pp. 269–279, 2012.
[8] M. Hwang, G. Kim, S. Kim, and N. S. Jeong, "Origami-inspired radiation pattern and shape reconfigurable dipole array antenna at c-band for cubesat applications," *IEEE Transactions on Antennas and Propagation*, vol. 69, no. 5, pp. 2697–2705, 2020.
[9] Q. He, T. Okajima, H. Onoe, A. Subagyo, K. Sueoka, and K. Kuribayashi-Shigetomi, "Origami-based self-folding of co-cultured nih/3t3 and hepg2 cells into 3d microstructures," *Scientific reports*, vol. 8, no. 1, pp. 1–7, 2018.
[10] M. Johnson, Y. Chen, S. Hovet, S. Xu, B. Wood, H. Ren, J. Tokuda, and Z. T. H. Tse, "Fabricating biomedical origami: a state-of-the-art review," *International journal of computer assisted radiology and surgery*, vol. 12, no. 11, pp. 2023–2032, 2017.
[11] A. G. Sorguç, I. Hagiwara, and S. A. Selçuk, "Origamics in architecture: A medium of inquiry for design in architecture," *Metu Journal of The Faculty of Architecture*, vol. 26, pp. 235–247, 2009.
[12] D. Rus and M. T. Tolley, "Design, fabrication and control of origami robots," *Nature Reviews Materials*, vol. 3, no. 6, pp. 101–112, 2018.
[13] D. Jeong and K. Lee, "Design and analysis of an origami-based three-finger manipulator," *Robotica*, vol. 36, no. 2, pp. 261–274, 2018.
[14] X. Liu, J. M. Gattas, and Y. Chen, "One-dof superimposed rigid origami with multiple states," *Scientific reports*, vol. 6, no. 1, pp. 1–9, 2016.
[15] T. Tachi, "Simulation of rigid origami," *Origami*, vol. 4, no. 08, pp. 175–187, 2009.
[16] Z. Xi and J.-M. Lien, "Folding rigid origami with closure constraints," in *International Design Engineering Technical Conferences and Computers and Information in Engineering Conference*, vol. 46377. American Society of Mechanical Engineers, 2014, p. V05BT08A052.
[17] W. Wu and Z. You, "Modelling rigid origami with quaternions and dual quaternions," *Proceedings of the Royal Society A: Mathematical, physical and engineering sciences*, vol. 466, no. 2119, pp. 2155–2174, 2010.
[18] J. Mitani, "A design method for 3d origami based on rotational sweep," *Computer-Aided Design and Applications*, vol. 6, no. 1, pp. 69–79, 2009.
[19] E. Peraza Hernandez, D. Hartl, and D. Lagoudas, "Design and simulation of origami structures with smooth folds," *Proceedings of the Royal Society A: Mathematical, Physical and Engineering Sciences*, vol. 473, no. 2200, p. 20160716, 2017.
[20] F. Wang, H. Gong, X. Chen, and C. Chen, "Folding to curved surfaces: A generalized design method and mechanics of origami-based cylindrical structures," *Scientific reports*, vol. 6, no. 1, pp. 1–10, 2016.
[21] X. Dang, F. Feng, P. Plucinsky, R. D. James, H. Duan, and J. Wang, "Inverse design of deployable origami structures that approximate a general surface," *International Journal of Solids and Structures*, vol. 234, p. 111224, 2022.
[22] T. Hull, "Unit origami as graph theory," in *V'Ann C, OrigamiUSA, editors. COET95. Proceedings of the 2nd International Conference on Origami in Education and Therapy. New York*. Citeseer, 1995, pp. 39–47.
[23] H. Huzita, "Axiomatic development of origami geometry," in *Proceedings of the First International Meeting of Origami Science and Technology, 1989*, 1989, pp. 143–158.
[24] K. Kasahara and T. Takahama, *Origami for the Connoisseur*. Japan Publications, 1998.
[25] T. Kawasaki, "Proceedings of the 1st international meeting of origami science and technology," 1989.
[26] J. Justin, "Résolution par le pliage de l'équation du troisieme degré et applications géométriques," in *Proceedings of the first international meeting of origami science and technology*. Ferrara, Italy, 1989, pp. 251–261.
[27] Z. He and S. D. Guest, "On rigid origami iii: local rigidity analysis," *Proceedings of the Royal Society A*, vol. 478, no. 2258, p. 20210589, 2022.
[28] M. Bern and B. Hayes, "The complexity of flat origami," in *SODA*, vol. 96. Atlanta, GA, 1996, pp. 175–183.
[29] K. Miura, "A note on intrinsic geometry of origami," *Research of pattern formation*, pp. 91–102, 1989.
[30] Y. Chen, H. Feng, J. Ma, R. Peng, and Z. You, "Symmetric waterbomb origami," *Proceedings of the Royal Society A: Mathematical, Physical and Engineering Sciences*, vol. 472, no. 2190, p. 20150846, 2016.
[31] J. Tang, M. Tian, C. Wang, X. Wang, and H. Mao, "A novel scheme of folding discretized surfaces of revolution inspired by waterbomb origami," *Mechanism and Machine Theory*, vol. 165, p. 104431, 2021.
[32] Y. Zhao, Y. Wei, Y. Jia, S. Li, M. Zhang, L. Zeng, Y. Yang, and J. Mitani, "Constructing foldable cylindrical surfaces via unfolded waterbomb origami units," *Journal of Computational Design and Engineering*, vol. 9, no. 4, pp. 1498–1510, 2022.

[33] K. Hayakawa and M. Ohsaki, "Form generation of rigid origami for approximation of a curved surface based on mechanical property of partially rigid frames," *International Journal of Solids and Structures*, vol. 216, pp. 182–199, 2021.
[34] L. Lu, X. Dang, F. Feng, P. Lv, and H. Duan, "Conical kresling origami and its applications to curvature and energy programming," *Proceedings of the Royal Society A*, vol. 478, no. 2257, p. 20210712, 2022.
[35] J. McInerney, B. G.-g. Chen, L. Theran, C. D. Santangelo, and D. Z. Rocklin, "Hidden symmetries generate rigid folding mechanisms in periodic origami," *Proceedings of the National Academy of Sciences*, vol. 117, no. 48, pp. 30 252–30 259, 2020.
[36] Z. He and S. D. Guest, "Approximating a target surface with 1-dof rigid origami," *arXiv preprint arXiv:1905.04773*, 2019.
[37] Y. Zhao, Y. Kanamori, and J. Mitani, "Design and motion analysis of axisymmetric 3d origami with generic six-crease bases," *Computer Aided Geometric Design*, vol. 59, pp. 86–97, 2018.
[38] C. Wan, G. Jing, R. Dai, and R. Zhao, "Local shape-preserving formation maneuver control of multi-agent systems: From 2D to 3D," in *Proceedings of the 60th IEEE Conference on Decision and Control*, 2021, pp. 6251–6257.
[39] E. D. Demaine and J. O'Rourke, *Geometric folding algorithms: linkages, origami, polyhedra*. Cambridge university press, 2007.
[40] L. Asimow and B. Roth, "The rigidity of graphs," *Transactions of the American Mathematical Society*, vol. 245, pp. 279–289, 1978.
[41] X. Chen, M.-A. Belabbas, and T. Başar, "Global stabilization of triangulated formations," *SIAM Journal on Control and Optimization*, vol. 55, no. 1, pp. 172–199, 2017.
[42] G. Jing, G. Zhang, H. W. Joseph Lee, and L. Wang, "Weak rigidity theory and its application to formation stabilization," *SIAM Journal on Control and optimization*, vol. 56, no. 3, pp. 2248–2273, 2018.
[43] J. W. Tolle, "Sequential quadratic programming," *Acta Numerica 1995: Volume 4*, vol. 4, pp. 1–51, 1995.
[44] P. E. Rutquist and M. M. Edvall, "Propt-matlab optimal control software," *Tomlab Optimization Inc*, vol. 260, no. 1, p. 12, 2010.

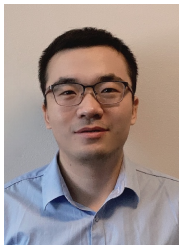

Gangshan Jing received the Ph.D. degree in Control Theory and Control Engineering from Xidian University, Xi'an, China, in 2018. From 2016 to 2017, he was a research assistant in Department of Applied Mathematics, at Hong Kong Polytechnic University. From 2018 to 2019, he was a postdoctoral researcher in Department of Mechanical and Aerospace Engineering, at Ohio State University. From 2019-2021, he was a postdoctoral researcher in Department of Electrical and Computer Engineering, at North Carolina State University. Since 2021 Dec, he has been a faculty member in School of Automation, Chongqing University, Chongqing. His research interests include distributed control, optimization, and machine learning for network systems.

Changhuang (Charlie) Wan is an assistant professor in Aerospace Science Engineering at Tuskegee University. He received bachelor and master degrees in Spacecraft Design and Engineering from Beihang University and his Ph.D. degree in in the Mechanical and Aerospace Engineering Department at The Ohio State University, Columbus, OH. His research interests include optimal control, numerical optimization, and autonomous systems.

Ran Dai is an associate professor in School of Aeronautics and Astronautics at Purdue University. She received her B.S. degree in Automation Science from Beihang University and her M.S. and Ph.D. degrees in Aerospace Engineering from Auburn University. Dr. Dai's research focuses on control of autonomous systems, numerical optimization, and networked dynamical systems. She is an associate editor of IEEE transaction on Aerospace and Electronic Systems, and a recipient of the National Science Foundation Career Award and NASA Early Faculty Career Award.

Mehran Mesbahi (Fellow, IEEE) received the Ph.D. degree in electrical engineering from the University of Southern California, Los Angeles, CA, USA, in 1996. He is currently a Professor of Aeronautics and Astronautics, an Adjunct Professor of Electrical and Computer Engineering and Mathematics, and the Executive Director of the Joint Center for Aerospace Technology Innovation, University of Washington, Seattle, WA, USA. His research interests include aerospace systems, control and learning, and networks. Dr. Mesbahi was the recipient of the NSF CAREER Award, the NASA Space Act Award, the UW Distinguished Teaching Award, the Graduate Instructor of the Year Award, and the UW College of Engineering Innovator Award.